www.nature.com/cr
www.cell-research.com

Cell Research

LETTER TO THE EDITOR

Cryo-EM structure of the AVP–vasopressin receptor 2–G_s signaling complex

Cell Research (2021) 31:932–934; https://doi.org/10.1038/s41422-021-00483-z

Dear Editor,

The highly conserved neuropeptides arginine vasopressin (AVP) and oxytocin (OT) signal through a family of Class A G protein-coupled receptors (GPCRs), the AVP receptors V1aR, V1bR and V2R and the OT receptor OXTR.[1,2] V2R is predominantly found in the kidney and plays a critical role in body fluid homeostasis.[2] Among all AVP and OT receptors, V2R is the only one that activates the heterotrimeric G_s family to induce cAMP accumulation (Supplementary information, Fig. S1). More than 200 mutations of the V2R gene have been linked to X-linked congenital nephrogenic diabetes insipidus (NDI) and nephrogenic syndrome of inappropriate antidiuresis (NSIAD).[2] V2R has also been the focus of intensive drug development efforts for urinary disorders.[2] Desmopressin (DDAVP), a peptide analog of AVP, is currently used to treat central diabetes insipidus and primary nocturnal enuresis. V2R antagonist drugs, the vaptans such as tolvaptan, are used to treat hyponatremia and autosomal dominant polycystic kidney disease (ADPKD).

Here, we report a cryo-EM structure of human AVP–V2R–G_s signaling complex at a global nominal resolution of 2.8 Å (Fig. 1a; Supplementary information, Fig. S2, Table S1). We used human V2R and human $G\alpha_s$, $G\beta_1$ and $G\gamma_2$ to assemble the complex. To facilitate cryo-EM structure determination, we modified human $G\alpha_s$ by replacing an N-terminal segment with N-terminal residues of $G\alpha_i$, so that the AVP–V2R–G_s complex can bind to two small antibody fragments (Supplementary information, Fig. S3). The clear cryo-EM map allowed modeling of entire AVP and the whole G_s heterotrimer except for the $G\alpha_s$ α-helical domain (AHD) in the structure. For the receptor, we modeled V2R from R32 to C342 except for residues E183–G188 in the extracellular loop 2 (ECL2), H150–W156 in the intracellular loop 2 (ICL2), and E242–S263 in the ICL3 due to poorly resolved maps of these regions.

The cyclic moiety of AVP formed by residues Cys1–Cys6 (residues in AVP are referred to by three-letter names, and residues in V2R and other proteins are referred to by one-letter names hereafter) is completely buried in the ligand-binding pocket of V2R, while the linear moiety formed by residues Pro7–Gly9 sticks towards the extracellular milieu (Fig. 1b). The main chain carbonyl group of AVP residue Gly9 forms a hydrogen bond with the main chain amine group of V2R residue R32. The side chain of AVP residue Arg8 forms cation–π interactions with the V2R residue W193 in ECL2. For the ring structure of AVP, the side chains of polar residues Tyr2 and Asn5 engage in polar interactions with the main chain groups of residues L312$^{7.40}$ and C192 of V2R, respectively. The V2R residue Q291$^{6.55}$ forms salt bridges with the side chain of Gln4 and the main amine group of Cys1 of AVP. Two aromatic residues of AVP, Tyr2 and Phe3, interact with V2R residues M120$^{3.33}$, M123$^{3.36}$, F287$^{6.51}$ and F288$^{6.52}$ to form a hydrophobic cluster at the bottom of the ligand-binding pocket, contributing to AVP binding. The disulfide bond of AVP together with Tyr2 also form hydrophobic interactions with V2R residues M311$^{7.39}$ and L312$^{7.40}$. Supporting the observed AVP binding pose in our structure, our mutagenesis data showed that individual mutations of W193, F287$^{6.51}$, and F288$^{6.52}$, could compromise or reduce AVP binding (Fig. 1c Supplementary information, Fig. S4). In addition, an NDI-causing mutation, F287V, has been shown to affect AVP binding.[3] Mutations of M123R/K, which potentially disrupt the hydrophobic interactions between V2R and AVP, have been identified as NDI-causing mutations.[4] Some NDI-causing mutations near the AVP-binding pocket including R104C, R106C and R181C may affect protein folding by interfering with the conserved disulfide bond between C192^{ECL2} and C112$^{3.25}$.[3,5] On the other hand, mutations of M123A, Q291A and L312A didn't seem to affect AVP binding significantly, suggesting minor roles of these residues in AVP binding (Fig. 1c, Supplementary information, Fig. S4).

Both AVP and OT can activate V2R, although the affinity of OT for V2R is ~500-fold lower than that of AVP.[6] AVP residues Phe3 and Arg8 are replaced by Ile3 and Leu8 in OT (Supplementary information, Fig. S1). The interactions mediated by Arg8 are important for AVP binding. Replacement of Arg8 of AVP with a D-isomer of arginine, which potentially disrupts its interactions with W193 of V2R, results in another V2R agonist, DAVP, with a ~40-fold lower affinity for V2R .[7] Therefore, the replacement of Arg8 by a Leu in OT may contribute to the lower affinity of OT. Interestingly, the AVP-binding pocket in V2R exhibits a highly positively charged environment, which is in contrast to the partially negatively charged ligand-binding pocket revealed by a crystal structure of inactive engineered OXTR with a small-molecule antagonist, retosiban[8] (Fig. 1d). Whether such distinct charge distributions contribute to the ligand selectivity of V2R and OXTR needs further investigation.

V2R in our structure represents an active conformation as a result of AVP binding and G_s coupling. A lack of inactive structures of V2R makes it difficult to speculate the receptor activation mechanism. Since OXTR is the closest phylogenetic GPCR neighbor of V2R with a 47% sequence identity in the 7TM domain (Supplementary information, Fig. S5a), we presumed a high structural similarity between these two receptors and we used the structure of inactive OXTR in our structural comparison analysis. Alignment of the active structure of V2R and the inactive structure of OXTR showed that the OXTR antagonist retosiban overlaps with a large part of the ring structure of AVP, suggesting a similar binding mode of OT in OXTR (Supplementary information, Fig. S5b). Compared to the inactive OXTR, there are large structural rearrangements of the cytoplasmic region of V2R, including a large outward displacement of TM6 and an inward movement of TM7 (Fig. 1d), which are characteristic of active Class A GPCRs.[9] In addition, ICL2 of the active V2R forms a short helix, while ICL2 of the inactive OXTR adopts a loop structure (Fig. 1d). This is analogous to the conformational change of ICL2 of the β_2-adrenergic receptor (β_2AR) from a loop structure to a short helix upon receptor activation.[10]

For Class A GPCRs, specific residues in the highly conserved F$^{6.44}$xxCW$^{6.48}$xxP motif in the core region of TM6 have been shown to undergo large conformational changes during receptor activation.[9]

Received: 11 October 2020 Accepted: 1 February 2021
Published online: 4 March 2021

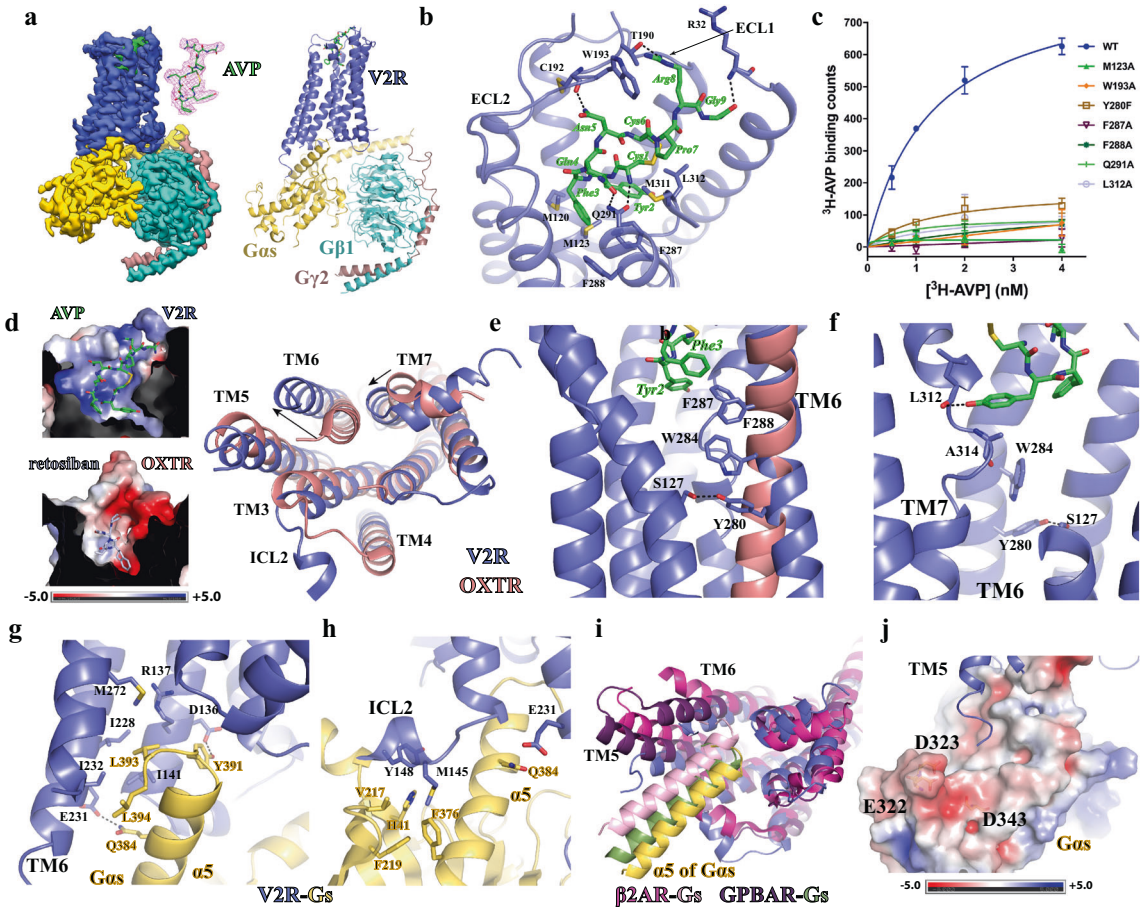

Fig. 1 Structure of the AVP–V2R–G_s complex. a Cryo-EM map of the complex and overall structure. The density of AVP shown as green sticks is colored in magenta. V2R, Gαs, Gβ and Gγ are colored in blue, dark yellow, cyan and brown, respectively. **b** Interactions between AVP and V2R. Residues in AVP are labeled with three-letter names while residues in V2R are labeled with one-letter names. Hydrogen bonds are shown as black dash lines. **c** Saturation binding results on wild-type V2R (WT) and mutants using ^{3}H-AVP. All V2R constructs were transiently expressed in HEK293 cells and the cells were used in the ligand binding assays. Expression of each construct was confirmed by cell surface staining as shown in Supplementary information, Fig. S4. Non-specific binding measured in the presence of an excess amount of AVP was subtracted. Each data point was shown as mean ± SD from 3 experiments. **d** Structural comparison of active V2R and inactive OXTR (PDB ID: 6TPK) at the extracellular regions (left panel) and the cytoplasmic regions (right panel). AVP and retosiban are shown as green and light blue sticks, respectively. The charge distribution of the ligand-binding pockets in both receptors is shown in the left panel. Residues in the middle regions of TM6 (**e**) and TM7 (**f**) involved in receptor activation. The kinked middle region of TM7 is also shown in **f**. V2R (blue) and G_s (dark yellow) interactions at the cytoplasmic cavity (**g**) and the ICL2 (**h**) of V2R. **i** Alignment of active structures of V2R (blue), β_2AR (magenta) and GPBAR (purple) at the cytoplasmic regions. The α5 of $G\alpha_s$ in the structures of G_s-coupled V2R, β_2AR and GPBAR is colored yellow, pink and dark green, respectively. **j** Negatively-charged region in $G\alpha_s$ that may be sampled by the arginine-rich region of V2R ICL3.

In particular, $W^{6.48}$ and $F^{6.44}$ form a 'transmission switch' linking receptor activation at the cytoplasmic region to the extracellular agonist binding.[9] However, in the V2R, while $W^{6.48}$ is conserved, $F^{6.44}$ is replaced by $Y280^{6.44}$ and it forms a hydrogen bond with $S127^{3.40}$ in TM3 (Fig. 1e). Thus, this residue may still play an important role in receptor activation. In the structure, two aromatic residues of AVP, Tyr2 and Phe3, form extensive π–π interactions with V2R residues $F287^{6.51}$ and $F288^{6.52}$ at the bottom of the ligand-binding pocket, which in turn pack against $W284^{6.48}$ (Fig. 1e). It is possible that conformational changes involving $F287^{6.51}$ and $F288^{6.52}$ upon AVP binding lead to conformational changes involving $W284^{6.48}$ and $Y280^{6.44}$ through steric effects to activate the receptor. In addition, there is an unusual deep kink around residue $A314^{7.42}$ of TM7 breaking TM7 into two non-continuous helices, likely due to the hydrogen bond between Tyr2 of AVP and the main chain carbonyl group of $L312^{7.40}$ (Fig. 1f). Such a kink brings the main chain carbonyl group of $A314^{7.42}$ close to $W284^{6.48}$ (Fig. 1f), possibly contributing to the conformational changes of $W284^{6.48}$ and $Y280^{6.44}$ to activate the receptor. In both scenarios, $W284^{6.48}$ and $Y280^{6.44}$ function as the conformational 'transmission switch'. Indeed, compared to the inactive OXTR, the outward shift of TM6 in V2R, which is the hallmark of GPCR activation,[11] starts at $W284^{6.48}$ (Fig. 1e). The unusual hydrogen bond between $S127^{3.40}$ and $Y280^{6.44}$ in the V2R may help to stabilize $Y280^{6.44}$ in the right conformation during the receptor activation process. Nevertheless, mutation Y280F didn't affect AVP binding (Fig. 1c, Supplementary information, Fig. S4). Whether it affects V2R activation needs further investigation. Noticeably, $Y^{6.44}$ is replaced by $F^{6.44}$ in the OXTR (Supplementary information, Fig. S4), implying certain divergent features of receptor activation for V2R and OXTR despite their close phylogenetic relationship.[1]

The main interaction sites between V2R and G_s are formed by residues in the cytoplasmic cavity of V2R and the α5 helix (α5) of $G\alpha_s$ (Fig. 1g). Two $G\alpha_s$ residues, L388 and L393, pack against V2R residues $I141^{3.54}$, $I228^{5.61}$, $I232^{5.65}$ and $M272^{6.36}$ to form extensive hydrophobic interactions. In addition, Y391 and Q383 of $G\alpha_s$ forms

polar interactions with V2R residues D136$^{3.49}$ and E231$^{5.64}$, respectively (Fig. 1g). Interestingly, D136$^{3.49}$ is a part of the conserved D$^{3.49}$R$^{3.50}$Y$^{3.51}$ (H138$^{3.51}$ in V2R) motif in Class A GPCRs. Previous studies showed that mutations of R137$^{3.50}$ had different effects on the V2R activity. In particular, R137L and R137C are gain-of-function mutations associated with NSIAD.[3] Based on our structure, R137L may result in additional hydrophobic interactions with Y391 and L393 of Gα$_s$ to further stabilize G$_s$ coupling. The mechanism for the gain of function of R137C mutation is not readily apparent.

In addition to residues in the cytoplasmic cavity, V2R residues M145$^{34.51}$ and Y148$^{34.54}$ in the short helix of ICL2 form a hydrophobic cluster with residues H41, V217, F219 and F376 of Gα$_s$, forming another V2R and G$_s$ interaction site (Fig. 1h). The structural integrity of ICL2 plays important roles in the G protein selectivity of vasopressin receptors.[12] For V2R, M145$^{34.51}$ is a critical structural determinant for the preference of G$_s$ over other G proteins. Mutations of M145$^{34.51}$ to W or L facilitate G$_q$ coupling to V2R.[12] On the other hand, mutations of M145$^{34.51}$ to A or G, which potentially abolish its hydrophobic interactions with Gα$_s$, did not change the G$_s$ signaling capacity of V2R.[10] This suggests that the interactions mediated by M145$^{34.51}$ are not critical for G$_s$ coupling to V2R.

For Class A GPCRs, two structures of the heterotrimeric G$_s$-coupled complexes, the β_2AR–G$_s$ and the bile acid receptor (GPBAR)–G$_s$ complexes, have been reported.[13,14] We compared the structure of the V2R–G$_s$ complex with those of G$_s$-coupled β_2AR and GPBAR complexes based on the alignment of receptors (Fig. 1i; Supplementary information, Fig. S6a). If we aligned the receptors, we observed that the relative orientations of G$_s$ to receptor were different and the α5 of Gα$_s$ inserted into receptor cavities in diverse conformations among all three structures, which were associated with distinct conformations of TM5 and TM6 of receptors (Fig. 1i). Relative to the α5 of Gα$_s$ in the V2R–G$_s$, the α5 of Gα$_s$ rotates ~6.5° in the GPBAR–G$_s$ and ~15.6° in the β_2AR–G$_s$, and shifts ~6 Å in the GPBAR–G$_s$ and ~10 Å in the β_2AR–G$_s$ measured at the Cα atom of Q390. If we only aligned the Gα$_s$ in these structures, while most regions in Gα$_s$ could be well aligned, the α5 and αN showed different conformations (Supplementary information, Fig. S6b). All these observations suggested diverse ways of G$_s$ coupling to Class A GPCRs. In addition, TM6 of V2R is more similar to that of GPBAR than to that of β_2AR (Fig. 1i). However, unlike GPBAR, a majority of ICL3 including arginine residues R243, R247, R249 and R251 are missing in the structure of V2R due to a lack of clear cryo-EM map (Fig. 1j). This arginine-rich domain has been shown to be important for V2R-induced G$_s$ signaling.[14] Nevertheless, a part of ICL3 following the C-terminal end of TM5 was modeled closely to the β4 and α4 of Gα$_s$. It is likely that the arginine-rich domain of ICL3 of V2R[14] samples a negatively-charged area of Gα$_s$ formed by E322 and D323 in i3 loop and D343 in α4 helix (Fig. 1j), similar to that observed in the structure of G$_s$-coupled GPBAR.[14]

In summary, we report the cryo-EM structure of the AVP–V2R–G$_s$ signaling complex. In the structure, the ring moiety of AVP inserts into a positively-charged binding pocket of V2R with the linear moiety extending towards the extracellular surface. AVP appears to activate V2R through conformational changes of the core region of 7TMs involving an aromatic cluster consisting of a non-conserved residue Y$^{6.44}$ in the middle of TM6 and the unusual kinked middle region of TM7. Similar to other GPCR–G protein signaling complexes, the α5 of Gα$_s$ inserts into the cytoplasmic cavity of V2R made accessible by the outward movement of TM6. In addition, our structure reveals a G$_s$ coupling mode distinct from that observed in structures of other G$_s$-coupled Class A GPCRs, highlighting the versatility of G$_s$ for coupling to Class A GPCRs.

DATA AVAILABILITY

The structural restraints ad coordinates of the AVP-V2R-Gs complex have been deposited in the Protein Data Bank (PDB: 7KH0) and the Electron Microscopy Data Bank (EMDB: EMD-22872).

ACKNOWLEDGEMENTS

We thank the Cryo-EM Facility Center of the Chinese University of Hong Kong, Shenzhen for providing technical support during EM image acquisition. Y.D. is supported by a grant from Science, Technology and Innovation Commission of Shenzhen Municipality (Project JCYJ20200109150019113), and in part by the Kobilka Institute of Innovative Drug Discovery and Presidential Fellowship at the Chinese University of Hong Kong, Shenzhen. C.Z. is supported by the grant R35GM128641 from the National Institutes of Health, the United States of America.

AUTHOR CONTRIBUTIONS

L.W. designed the expression constructs and purified the AVP–V2R–G$_s$ complex. L.W. and S.C. prepared the samples for cryo-EM data collection. L.W. and J.X. performed screening of cryo-EM grids and data collection. J.X. processed cryo-EM data. L.W. built the model. D.S. and C.Z. refined the structure model. Z.L., Q.L. and S.C. assisted cryo-EM data collection and processing. H.L. assisted cloning. Y.D. and C.Z. supervised all studies, and C.Z. wrote the manuscript with Y.D., L.W. and J.X.

ADDITIONAL INFORMATION

Supplementary information The online version contains supplementary material available at https://doi.org/10.1038/s41422-021-00483-z.

Competing interests: The authors declare no competing interests.

Lei Wang[1,2], Jun Xu[1], Sheng Cao[1], Dapeng Sun[2], Heng Liu[2], Qiuyuan Lu[1], Zheng Liu[1], Yang Du[1] and Cheng Zhang[2]
[1]Kobilka Institute of Innovative Drug Discovery, School of Life and Health Sciences, Chinese University of Hong Kong, Shenzhen, Guangdong 518172, China and [2]Department of Pharmacology and Chemical Biology, School of Medicine, University of Pittsburgh, Pittsburgh, PA 15213, USA
These authors contributed equally: Lei Wang, Jun Xu.
Correspondence: Yang Du (yangdu@cuhk.edu.cn) or Cheng Zhang (chengzh@pitt.edu)

REFERENCES

1. Fredriksson, R., Lagerstrom, M. C., Lundin, L. G. & Schioth, H. B. *Mol. Pharmacol.* **63**, 1256–1272 (2003).
2. Juul, K. V., Bichet, D. G., Nielsen, S. & Norgaard, J. P. *Am. J. Physiol. Renal. Physiol.* **306**, F931–F940 (2014).
3. Makita, N., Manaka, K., Sato, J. & Iiri, T. *Vitam. Horm.* **113**, 79–99 (2020).
4. Sasaki, S., Chiga, M., Kikuchi, E., Rai, T. & Uchida, S. *Clin. Exp. Nephrol.* **17**, 338–344 (2013).
5. Miyakoshi, M., Kamoi, K., Uchida, S. & Sasaki, S. *Endocr. J.* **50**, 809–814 (2003).
6. Tahara, A. et al. *Br. J. Pharmacol.* **125**, 1463–1470 (1998).
7. Cotte, N. et al. *J. Biol. Chem.* **273**, 29462–29468 (1998).
8. Waltenspuhl, Y., Schoppe, J., Ehrenmann, J., Kummer, L. & Pluckthun, A. *Sci. Adv.* **6**, eabb5419 (2020).
9. Weis, W. I. & Kobilka, B. K. *Annu. Rev. Biochem.* **87**, 897–919 (2018).
10. Rasmussen, S. G. et al. *Nature* **469**, 175–180 (2011).
11. Manglik, A. & Kruse, A. C. *Biochemistry* **56**, 5628–5634 (2017).
12. Erlenbach, I. et al. *J. Biol. Chem.* **276**, 29382–29392 (2001).
13. Rasmussen, S. G. et al. *Nature* **477**, 549–555 (2011).
14. Yang, F. et al. *Nature* **587**, 499–504 (2020).